Available online at www.sciencedirect.com
ScienceDirect
Journal of the European Ceramic Society 27 (2007) 4473–4478
www.elsevier.com/locate/jeurceramsoc

Effects of Mg/Fe substitution on perovskite stabilization and dielectric properties of $Pb(Zn_{1/2}W_{1/2})O_3$

Woo-Joon Lee, Jee-Su Kim, Nam-Kyoung Kim *

Department of Inorganic Materials Engineering, Kyungpook National University, Daegu 702-701, Republic of Korea

Received 10 January 2007; received in revised form 5 March 2007; accepted 16 March 2007
Available online 30 May 2007

Abstract

The effects of compositional modification by substituting Mg or Fe for Zn on the perovskite formation, crystallographic aspects, and dielectric properties of $Pb(Zn_{1/2}W_{1/2})O_3$ were investigated. Microstructural evolutions in the sintered ceramics were also examined. Stabilization of the perovskite structure was accomplished by a much smaller concentration of Mg substitution. Lattice parameters of the perovskite decreased with increasing substituent fractions in general. By contrast, the permittivity values increased significantly with increasing Mg/Fe substitution.

Keywords: Powders-solid state reaction; X-ray methods; Dielectric properties; Perovskites; $Pb(Zn,W)O_3$ (PZW)

1. Introduction

Lead magnesium tungstate $Pb(Mg_{1/2}W_{1/2})O_3$ (PMW) is an antiferroelectric compound with a 1:1-ordered configuration in the B-site sublattice.[1–5] By contrast, lead iron tungstate $Pb(Fe_{2/3}W_{1/3})O_3$ (PFW) is a relaxor ferroelectric with a disordered arrangement of Fe and W in the octahedral lattice sites.[5–10] Both PMW and PFW have been synthesized to a perovskite structure quite easily through solid-state reaction methods. Meanwhile, formation of the perovskite in lead zinc tungstate $Pb(Zn_{1/2}W_{1/2})O_3$ (PZW) has not been reported yet, despite the fact that the stoichiometry of PZW is identical to that of PMW. Actually, only mixed phases of Pb_2WO_5 and ZnO resulted.[11] It should be noted that the expression of $Pb(Zn_{1/2}W_{1/2})O_3$ (as well as PZW) in the present paper does not necessarily indicate the formability of a perovskite structure, but simply denotes the composition instead.

In the present study, therefore, the perovskite stabilization in $Pb(Zn_{1/2}W_{1/2})O_3$ was attempted by substituting the octahedral lattice component of Zn by isovalent Mg. In addition, the effect of the aliovalent Fe replacement for Zn was also investigated and the results are compared. Changes in the phase development, crystal symmetry, and dielectric properties as well as microstructural evolutions were examined. During the powder preparation stage, a B-site precursor method[9,12] (synonymous to the columbite process[13]) was adopted in order to promote the perovskite stabilization.

2. Experimental

The Mg- and Fe-substituted compositions can be expressed as $(1-x)Pb(Zn_{1/2}W_{1/2})O_3$–$xPb(Mg_{1/2}W_{1/2})O_3$ and $(1-y)Pb(Zn_{1/2}W_{1/2})O_3$–$yPb(Fe_{2/3}W_{1/3})O_3$ (or $(1-x)$PZW–xPMW and $(1-y)$PZW–yPFW), which will be referred to as PZW–xMg and PZW–yFe, respectively. The values of x and y were selected up to 1.0 at regular intervals of 0.2. Starting materials were oxide powders of PbO (99.5% purity), ZnO (99.8%), MgO (99.9%), Fe_2O_3 (99.99%), and WO_3 (>99%). Moisture contents of the raw chemicals and of the B-site precursor powders were measured and introduced into the batch calculation in order to maintain stoichiometries as closely to the nominal values as possible.

B-site precursor powders of $(1-x)(Zn_{1/2}W_{1/2})O_2$–$x(Mg_{1/2}W_{1/2})O_2$ and $(1-y)(Zn_{1/2}W_{1/2})O_3$–$y(Fe_{2/3}W_{1/3})O_2$ were prepared by reacting constituent chemicals in appropriate ratios for 2 h each at 650–750 and 650–850 °C (depending on composition), respectively. The powders were wet-milled, dried, and calcined again at 650–750 and 650–1000 °C for additional 2 h so as to promote the phase development. PbO was then added to the prepared powders (also in stoichiometric proportions) and

* Corresponding author. Tel.: +82 53 950 5636; fax: +82 53 950 5645.
E-mail address: nkkim@knu.ac.kr (N.-K. Kim).

0955-2219/$ – see front matter © 2007 Elsevier Ltd. All rights reserved.
doi:10.1016/j.jeurceramsoc.2007.03.028

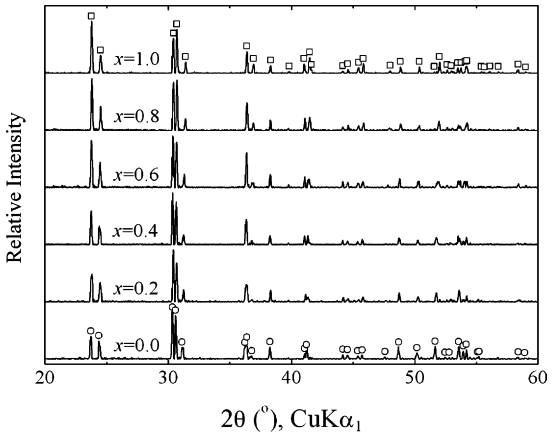

Fig. 1. X-ray diffraction results of $(1-x)(Zn_{1/2}W_{1/2})O_2$–$x(Mg_{1/2}W_{1/2})O_2$. (◯) $ZnWO_4$ and (□) $MgWO_4$.

the whole batches were wet-milled, dried, and calcined at 750 °C (system PZW–*x*Mg) and 750–800 °C (system PZW–*y*Fe) for 2 h each with intermediate milling and drying steps. Prepared powders were examined by an X-ray diffractometry (XRD, Cu Kα, monochromator) in order to identify the phases formed.

The powders (with 2 wt.% aqueous solution of polyvinyl alcohol binder) were isostatically pressed into pellets. The preformed compacts were fired at 875–925 and 775–875 °C (with a soaking time of 1 h) for the two systems, respectively. Volatilization of PbO during the sintering stage was suppressed by employing a multiple-enclosure crucible setup[14] with identical composition powders surrounding the pellets. Major surfaces of the sintered ceramics were polished and electroded by Au sputtering. Dielectric properties of the ceramics were measured on cooling using an impedance analyzer under weak-field (∼1 V_{rms}/mm) low-frequency (1–1000 kHz) conditions. After Au coating, microstructures of the fractured ceramics were examined by scanning electron microscopy (SEM).

3. Results and discussion

XRD results of the two precursor systems are presented in Figs. 1 and 2. In $(1-x)(Zn_{1/2}W_{1/2})O_2$–$x(Mg_{1/2}W_{1/2})O_2$ (Fig. 1), the only phase present was a wolframite solid solution $(Zn,Mg)WO_4$, which formed between the two end members. The development of continuous solubility in the entire composition range is undoubtedly attributed to the identical wolframite structures of $ZnWO_4$ (ICDD No. 15–774) and $MgWO_4$ (ICDD No. 27–789). In $(1-y)(Zn_{1/2}W_{1/2})O_2$–$y(Fe_{2/3}W_{1/3})O_2$ (Fig. 2), by contrast, the wolframite structure of $ZnWO_4$ was observable at $y \leq 0.6$, whereas Fe_2WO_6 (ICDD No. 20–539) was detected at $0.4 \leq y$, with the two phases coexisting at intermediate compositions of $y = 0.4$ and 0.6. The limited solubility resulted from the substantially different crystal structures in the end components of $ZnWO_4$ and Fe_2WO_6.

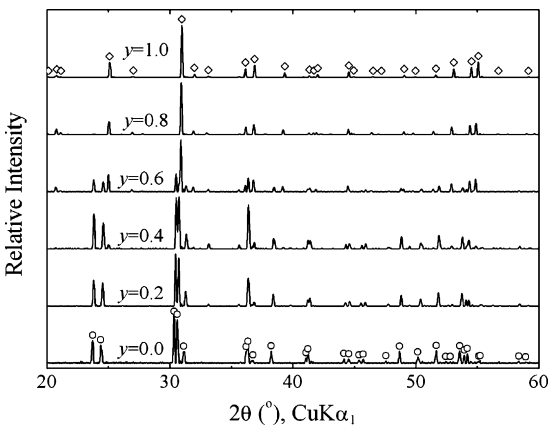

Fig. 2. X-ray diffraction results of $(1-y)(Zn_{1/2}W_{1/2})O_2$–$y(Fe_{2/3}W_{1/3})O_2$. (◯) $ZnWO_4$ and (◊) Fe_2WO_6.

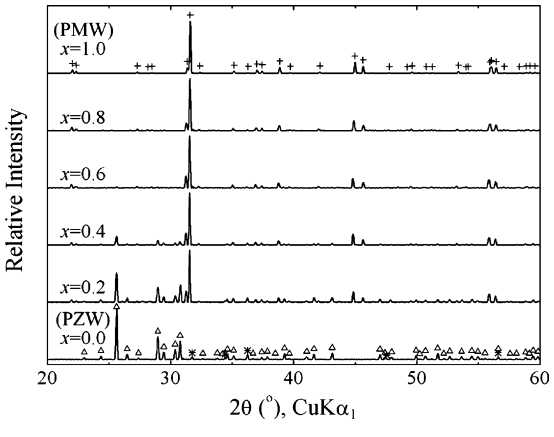

Fig. 3. XRD traces of $(1-x)$PZW–xPMW. (△) Pb_2WO_5(I), (∗) ZnO, and (+) perovskite.

X-ray diffraction traces of PZW–*x*Mg and PZW–*y*Fe are contrasted in Figs. 3 and 4. In $PbO + (1/2)ZnWO_4$ (x, $y = 0.0$, i.e., PZW), the result was only a biphasic mixture of Pb_2WO_5 and ZnO. It has been argued in the literature[11] that the B-site precursor component $ZnWO_4$ decomposed into ZnO and WO_3, followed by recombination of the latter with PbO to form Pb_2WO_5 (ICDD No. 36–1495), thus leaving ZnO as a by-product. Lack of the perovskite formation in PZW (even by the B-site precursor method) seems to be closely associated with the highly covalent nature of Zn,[15] when compared with the ready formability in PMW with more ionic Mg. The failure may also

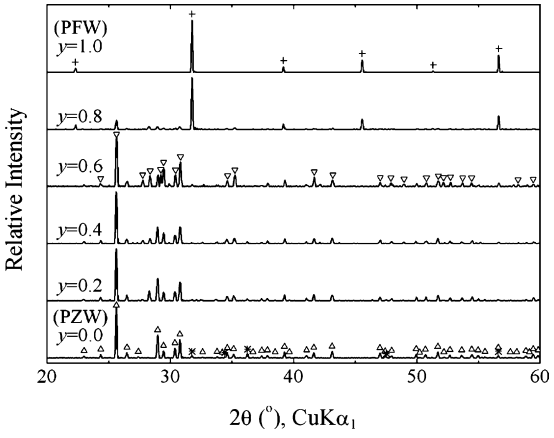

Fig. 4. XRD traces of $(1-y)$PZW–yPFW. (△) Pb_2WO_5(I), (▽) Pb_2WO_5(II), (∗) ZnO, and (+) perovskite.

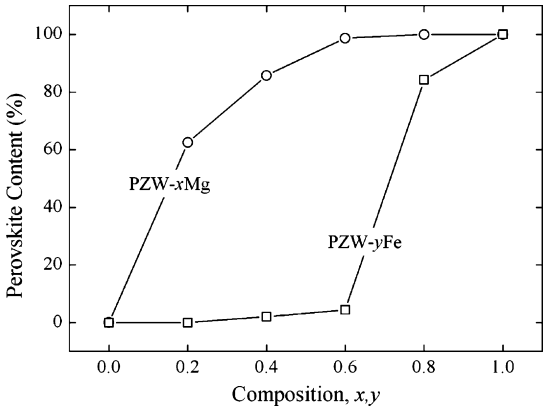

Fig. 5. Perovskite formation yields in the two systems.

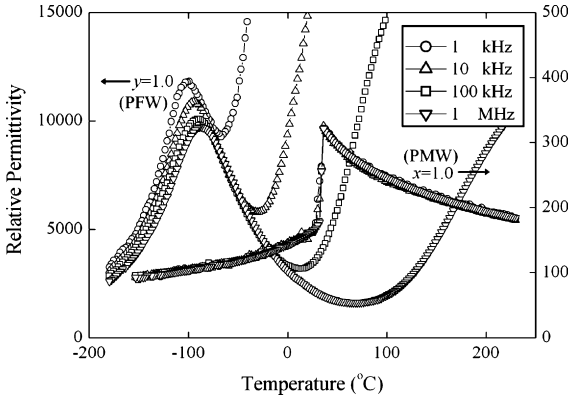

Fig. 7. Dependence of the permittivity values of x, $y = 1.0$ upon measurement frequency.

be attributed to the somewhat larger size of Zn than Mg, the ionic radii[16] of which are 0.0740 and 0.0720 nm, respectively.

With increasing substituent fractions in system PZW–xMg (Fig. 3), the biphasic result changed steadily to the patterns of the perovskite PMW (ICDD No. 46–1499). In system PZW–yFe (Fig. 4), however, the trends are somewhat complicated in that the peaks of Pb_2WO_5 changed gradually to those of another polymorph (ICDD No. 37–306) at low-to-medium substituent fractions, prior to the development of the perovskite PFW (ICDD No. 40–374). Therefore, the two polymorphic forms were differentiated as Pb_2WO_5(I) and Pb_2WO_5(II) in the figure. By comparing the two data sets, it can be concluded that the perovskite structure started to develop at a much lower substitution level in system PZW–xMg ($x = 0.2$).

In order to quantitatively compare the perovskite stabilization in the two systems, the perovskite development yields were estimated by intensity comparison among the strongest peaks of coexisting phases and the results are plotted in Fig. 5. As was shown for x, $y = 0.0$ (Figs. 3 and 4), the perovskite structure did not develop at all (perovskite content = 0%). Then, the perovskite content increased rapidly to 62% ($x = 0.2$) in system PZW–xMg. The values further increased with increasing Mg fractions and reached a virtual completion (perovskite yield > 99%) at $x \geq 0.6$. In the PZW–yFe system, by contrast, the perovskite yields were only < 5% at $y \leq 0.6$, which increased to

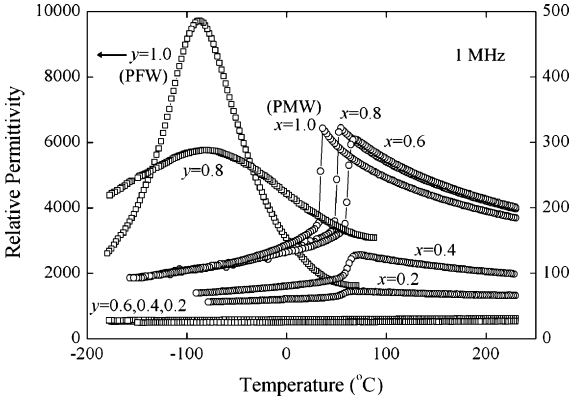

Fig. 8. Permittivity values of systems PZW–xMg and PZW–yFe. All data points (except for those of $y = 1.0$) refer to the right ordinate.

84% ($y = 0.8$) and > 99% ($y = 1.0$). It turned out from the much faster increases in PZW–xMg, therefore, that the substitution of Zn in PZW by isovalent Mg is more efficient in the perovskite stabilization, when compared with the results by aliovalent Fe (system PZW–yFe). As for the 'under-formation' of a perovskite phase in system PZW–xMg ($x = 0.2$ and 0.4), any second crystalline phase was not observed, in comparison with the results of PZW–yFe. This implies that a significant portion of the ceramic

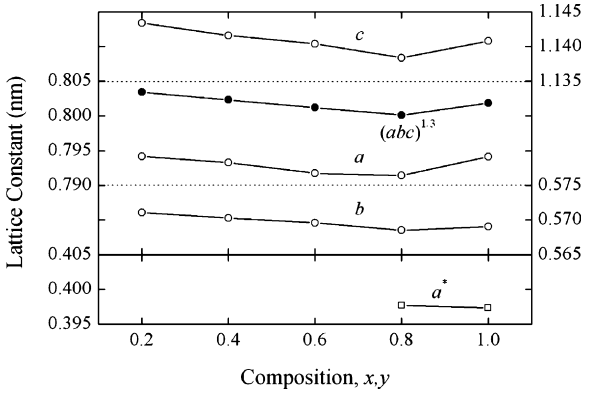

Fig. 6. Lattice parameters of a perovskite structure with a, b, and c for PZW–xMg and a* for PZW–yFe.

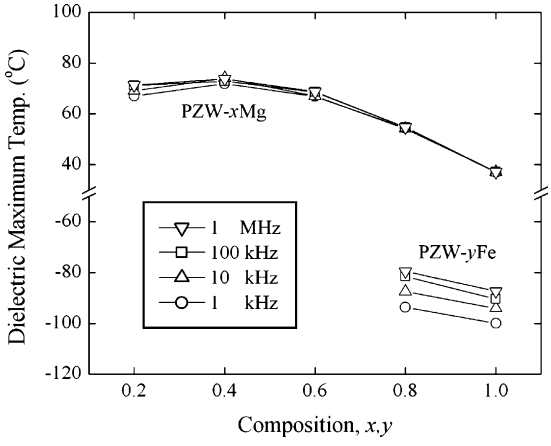

Fig. 9. Variations of the dielectric maximum temperatures with compositional and frequency changes.

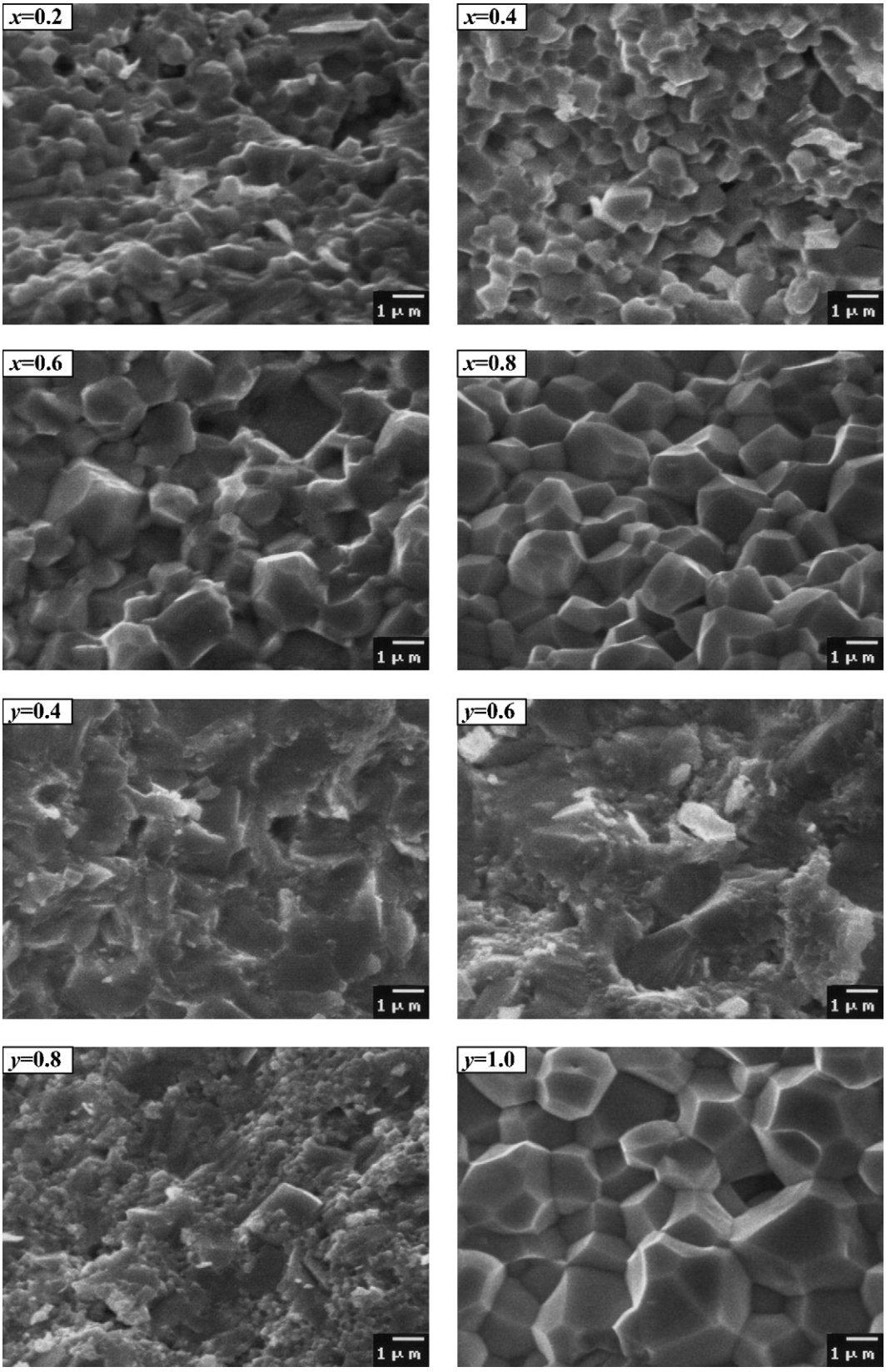

Fig. 10. SEM images of the fractured ceramics of the two systems ($x = 0.2$–0.8; $y = 0.4$–1.0).

in PZW–xMg may be an imperfectly crystalline (i.e., amorphous) state. Hence, there is a potential for optimization of the calcination/sintering conditions for the compositions in order to increase the perovskite yield, which will be the focus of future work.

Lattice parameters of the perovskite structure in the two systems were estimated from the XRD profiles and the results are displayed in Fig. 6. The diffraction patterns of the two systems could be indexed in terms of orthorhombic and cubic unit cells, respectively. All of the lattice parameters (a, b, and c) in system PZW–xMg decreased at similar rates in the composition range of $x = 0.2$–0.8, thus resulting in a steady decrease in the average values of $(a\,b\,c)^{1/3}$ from 0.8034 to 0.8001 nm. Finally at $x = 1.0$ (PMW), however, the values increased somewhat to 0.8018 nm, quite close to the reported data (ICDD Nos. 46–1499 and 80–107). However, the increase is somewhat different to the gradually decreasing trends in the other composition ranges, which need to be investigated further. Similarly, the lattice parameter of $a = 0.3977$ nm ($y = 0.8$) in system PZW–yFe also decreased slightly to 0.3973 nm ($y = 1.0$, PFW), which is fairly consistent with the reported value (ICDD No. 40–374). The general trends of decreasing lattice parameters with increasing substituent fractions can be explained by considering the weight-averaged effective ionic radii[16] of $Zn_{1/2}W_{1/2}$, $Mg_{1/2}W_{1/2}$, and $Fe_{2/3}W_{1/3}$ complexes: 0.067, 0.066, and 0.063 nm, respectively.

Permittivity values (ε_r) of x, $y = 1.0$ (i.e., PMW and PFW) are compared in Fig. 7, whereby two very different modes of phase transition were demonstrated. The transition modes of $x = 1.0$ were quite sharp, whereas those of $y = 1.0$ were rather diffuse. Values of the maximum permittivity ($\varepsilon_{r,max}$) and corresponding temperature (T_{max}) of $x = 1.0$ were $\varepsilon_{r,max} = 330$ ($T_{max} = 37\,^{\circ}C$), regardless of the measurement frequency. The sharp spectra with rather low values of $\varepsilon_{r,max}$ are basic features of antiferroelectric materials, including PMW. By contrast, corresponding values of $y = 1.0$ were $\varepsilon_{r,max} = 11{,}800$ ($T_{max} = -100\,^{\circ}C$), 10,900 ($-94\,^{\circ}C$), 10,100 ($-90\,^{\circ}C$), and 9700 ($-87\,^{\circ}C$) at 1–1000 kHz, showing typical behavior of frequency-dependent dielectric relaxation. Meanwhile, the permittivity values of $y = 1.0$ increased again in the paraelectric temperature ranges. Such recurrent increases were often observed in $Pb(Fe_{1/2}Ta_{1/2})O_3$,[17,18] $Pb(Fe_{1/2}Nb_{1/2})O_3$,[19,20] and $Pb(Fe_{2/3}W_{1/3})O_3$,[9,17] which were explained by the interfacial polarization at the thin grain boundary layers[18,19,21] or by oxygen vacancies associated with the valence change in Fe.[22]

Permittivity values of the entire compositions are shown in Fig. 8, where the result of x, $y = 0.0$ (PZW) could not be included, as the powder compacts were not sintered properly. All of the compositions in system PZW–xMg developed sharp maximum peaks with magnitudes of 70 ($x = 0.2$), 130 ($x = 0.4$), 300 ($x = 0.6$), 320 ($x = 0.8$), and 330 ($x = 1.0$, PMW). In system PZW–yFe, by contrast, the permittivity values for $y = 0.2$–0.6 simply increased steadily with increasing temperature, i.e., without any development of maximum peaks. This reflects the formation of two phases for these chemical compositions (Fig. 2). Room-temperature values of the three compositions were only 25–30 with average gradients of 220–280 ppm/K. At higher values of y, however, diffuse peaks were developed, the magnitudes of which were 290 ($y = 0.8$) and 9700 ($y = 1.0$, PFW). The much lower values at $x = 0.2$, 0.4 and $y = 0.8$ (compared with those of the remaining compositions) can be explained by the incomplete stabilization of perovskite phase with low yields (Fig. 5). Meanwhile, the sharp ($x = 1.0$) and diffuse ($y = 1.0$) phase transition modes in Fig. 7 were preserved throughout the entire compositions in each system, except for the two-phase region $y = 0.2$–0.6.

Dielectric maximum temperatures (T_{max}) of the ceramics in the two systems are plotted in Fig. 9. The values in system PZW–xMg changed rather gradually: 71, 73, 69, 55, and 37 °C (1 MHz) in the composition range $x = 0.2$–1.0 with the highest values at $x = 0.4$. The irregular variation can be explained by the coexistence of Pb_2WO_5, by which the T_{max} values were lowered especially at low values of x. From the apparently lower T_{max} values, therefore, it can be deduced that the values of ε_r for Pb_2WO_5 are rather low. Meanwhile, the degree of frequency-dependent dispersion ($\Delta T_{max} = T_{max,1\,MHz} - T_{max,1\,kHz}$) was only 4 °C ($x = 0.2$), which decreased gradually to negligible values ($\ll 1\,^{\circ}C$) at $x = 0.8$ and 1.0. By contrast, the dispersion in system PZW–yFe was quite substantial, $\Delta T_{max} = 14\,^{\circ}C$ ($y = 0.8$) and 13 °C ($y = 1.0$). Moreover, the values of T_{max} in system PZW–yFe were much lower than those in system PZW–xMg, resulting from the inherently lower T_{max} values of PFW (-95 to $-90\,^{\circ}C$[23–26]), as compared with 35–40 °C of PMW.[1,3,23–27]

Fractomicrographs of the ceramics are presented in Fig. 10. At low values of x (system PZW–xMg), the microstructures were composed of incipient polyhedral grains with scattered pores, supporting the possibilities of imperfectly crystalline state. With increasing x, however, the microstructures changed gradually to typical perovskite grains of multifaceted morphology. Finally at $x = 0.8$ (perovskite yield = 100%), only perovskite grains (average size = 2.5 μm) with intergranular fracture modes were observed. The micrograph of $x = 1.0$ was similar to that of $x = 0.8$, except for a slightly larger grain size of 3.1 μm, hence was not shown. In system PZW–yFe, only ill-defined grains with transgranular fracture modes were observable at low-to-medium values of y. The development of polyhedral perovskite grains was accomplished only at $y = 1.0$ (perovskite yield = 99.9%) with an average grain size of 3.4 μm. The micrographs in the two systems are generally consistent with the perovskite formation yields in Fig. 5.

4. Summary

Complete solubility in the entire composition range of $(Zn_{1/2}W_{1/2})O_2$–$(Mg_{1/2}W_{1/2})O_2$ resulted from the isostructural nature in the end components. By contrast, substantially different structures between the end components of $(Zn_{1/2}W_{1/2})O_2$–$(Fe_{2/3}W_{1/3})O_2$ resulted in mixed phases in the intermediate compositions. After the addition of PbO and appropriate calcination, Mg substitution for Zn in PZW was found to be much more effective in the perovskite stabilization, when compared with the Fe-substituted case. Lattice parameters of the perovskite structure decreased generally with increasing fractions in the two systems, regardless of the substituent species. Frequency-dependent dielectric relaxation behavior (along with

diffuse modes in the phase transition) was observable in system PZW–*y*Fe, whereas the spectra in system PZW–*x*Mg were quite sharp with little dispersion. Permittivity values increased substantially with increasing fractions of Mg and Fe in the two systems. Fractomicrographs of the ceramics are basically consistent with the perovskite formation results.

References

1. Zhang, X.-W., Wang, Q. and Gu, B. L., Study of the order-disorder transition in A(B'B")O_3 perovskite type ceramics. *J. Am. Ceram. Soc.*, 1991, **74**, 2846–2850.
2. Uchikoba, F. and Sawamura, K., JIS YB lead complex perovskite ferroelectric material. *Jpn. J. Appl. Phys.*, 1992, **31**, 3124–3127.
3. Ochi, A., Mori, T. and Furuya, M., Dielectric properties and crystal structures of entire compositions in the ternary system $Pb(Mg_{1/2}W_{1/2})O_3$–$Pb(Ni_{1/3}Nb_{2/3})O_3$–$PbTiO_3$. In *Proceedings on the 8th IEEE International Symposium on Application of Ferroelectrics*, 1992, pp. 66–69.
4. Choo, W. K., Kim, H. J., Yang, J. H., Lim, H., Lee, J. Y., Kwon, J. R. *et al.*, Crystal structure and B-site ordering in antiferroelectric $Pb(Mg_{1/2}W_{1/2})O_3$, $Pb(Co_{1/2}W_{1/2})O_3$, and $Pb(Yb_{1/2}Nb_{1/2})O_3$. *Jpn. J. Appl. Phys.*, 1993, **32**, 4249–4253.
5. Agranovskaya, A. I., Physical–chemical investigation of the formation of complex ferroelectrics with the perovskite structure. *Bull. Acad. Sci. USSR Phys. Ser.*, 1960, **24**, 1271–1277.
6. Uchino, K. and Nomura, S., Phenomenological theory of ferroelectricity in solid solution systems $Pb(Fe_{2/3}W_{1/3})O_3$–$Pb(M_{1/2}W_{1/2})O_3$ (M = Mn, Co, Ni). *Jpn. J. Appl. Phys.*, 1979, **18**, 1493–1497.
7. Yasuda, N., Fujimoto, S. and Tanaka, K., Dielectric properties of $Pb(Fe_{2/3}W_{1/3})O_3$ under pressure. *J. Phys. D: Appl. Phys.*, 1985, **18**, 1909–1917.
8. Lu, C.-H., Ishizawa, N., Shinozaki, K., Mizutani, N. and Kato, M., Synthesis and cell refinement of $PbFe_{2/3}W_{1/3}O_3$ and pyrochlore-related phase in the Pb–Fe–W–O system. *J. Mater. Sci. Lett.*, 1988, **7**, 1078–1079.
9. Lee, B.-H., Kim, N.-K., Kim, J.-J. and Cho, S.-H., Perovskite formation sequence by B-site precursor method and dielectric properties of PFW–PFN ceramics. *Ferroelectrics*, 1998, **211**, 233–247.
10. Jun, S. G. and Kim, N. K., Dielectric properties of PFW–PMN relaxor system prepared by B-site precursor method. *J. Mater. Sci.*, 2000, **35**, 2093–2097.
11. Lee, W.-J. and Kim, N.-K., Phase developmental stages in $Pb(Mg_{1/2}W_{1/2})O_3$ and $Pb(Zn_{1/2}W_{1/2})O_3$ via B-site precursor route. *Mater. Res. Bull.*, submitted for publication.
12. Ananta, S. and Thomas, N. W., A modified two-stage mixed oxide synthetic route to lead magnesium niobate and lead iron niobate. *J. Eur. Am. Ceram. Soc.*, 1999, **19**, 155–163.
13. Swartz, S. L. and Shrout, T. R., Fabrication of perovskite lead magnesium niobate. *Mater. Res. Bull.*, 1982, **17**, 1245–1250.
14. Chae, M.-C., Kim, N.-K., Kim, J.-J. and Cho, S.-H., Preparation and dielectric properties of $Pb[(Mg_{1/3}Ta_{2/3}),(Zn_{1/3}Nb_{2/3})]O_3$ relaxor ceramics. *Ferroelectrics*, 1998, **211**, 25–39.
15. Smith, W. F., *Principles of Materials Science and Engineering* (*2nd ed.*). McGraw-Hill, Singapore, 1990, p. 37.
16. Shannon, R. D., Revised effective ionic radii and systematic studies of interatomic distances in halides and chalcogenides. *Acta Crystallogr.*, 1976(A32), 751–767.
17. Smolenskii, G. A., Agranovskaya, A. I. and Isupov, V. A., New ferroelectrics of complex composition. III. Pb_2MgWO_6, $Pb_3Fe_2WO_9$, and Pb_2FeTaO_6. *Sov. Phys.-Solid State*, 1959, **1**, 907–908.
18. Lee, B.-H., Kim, N.-K., Kim, J.-J. and Cho, S.-H., Dielectric characteristics of $Pb[Fe_{1/2}(Ta,Nb)_{1/2}]O_3$ perovskite ceramic system. *J. Kor. Phys. Soc.*, 1998, **32**, S978–S980.
19. Ichinose, N., Kato, N. and Yamaguchi, K., Anomalous dielectric properties in $Pb(Fe_{1/2}Nb_{1/2})O_3$ ceramics. In *Ceramic Transactions, Dielectric Ceramics: Processing, Properties, and Applications*, *Vol. 32*, ed. K. M. Nair, J. P. Guha and A. Okamoto. American Ceramic Society, 1993, pp. 211–220.
20. Jun, S.-G., Kim, N.-K., Kim, J.-J. and Cho, S.-H., Synthesis of perovskite ceramics PMN–PFN via B-site precursors and their dielectric properties. *Mater. Lett.*, 1998, **34**, 336–340.
21. Goda, K. and Kuwabara, M., Another dielectric anomaly in $(PbLa)TiO_3$ ceramics above the curie temperature. In *Ceramic Transactions, Ceramic Powder Science IV*, *Vol. 22*, ed. S.-I. Hirano. American Ceramic Society, 1991, pp. 503–508.
22. Ichinose, N. and Kato, N., Dielectric properties of $Pb(Fe_{1/2}Nb_{1/2})O_3$-based ceramics. *Jpn. J. Appl. Phys.*, 1994, **33**, 5326–5423.
23. Uchino, K. and Nomura, S., Crystallographic and dielectric properties in the solid solution systems $Pb(Fe_{2/3}W_{1/3})O_3$–$Pb(Mg_{1/3}Ta_{2/3})O_3$ and $Pb(MgW)_{1/2}O_3$–$Pb(FeTa)_{1/2}O_3$. *J. Phys. Soc. Jpn.*, 1976, **41**, 542–547.
24. Sakabe, Y., Recent progress on multilayer ceramic capacitors. In *Proc. MRS Int. Mtg. Adv. Mater., Vol. 10, Multilayers*, ed. M. Doyama, S. Somiya and R. P. H. Chang. MRS, 1989, pp. 119–129.
25. Shrout, T. R. and Dougherty, J. P., Lead-based $Pb(B_1, B_2)O_3$ relaxors vs. $BaTiO_3$ dielectrics for multilayer capacitors. In *Ceramic Transactions, Vol. 8. Ceramic Dielectrics: Composition, Processing, and Properties*, ed. H. C. Ling and M. F. Yan. American Ceramic Society, 1990, pp. 3–19.
26. Yamashita, Y., PZN-based Relaxors for MLCCs. *Am. Ceram. Soc. Bull.*, 1994, **73**, 74–80.
27. Furuya, M., Mori, T., Ochi, A., Saito, S. and Takahashi, S., Dielectric properties and crystal structures in ternary system $Pb(Mg_{1/2}W_{1/2})O_3$–$Pb(Ni_{1/3}Nb_{2/3})O_3$–$PbTiO_3$ ceramics. *Jpn. J. Appl. Phys.*, 1992, **31**, 3139–3143.